Photochemistry and Photobiology
The official journal of the American Society of Photobiology

Quantifying direct DNA damage in the basal layer of skin exposed to UV radiation from sunbeds

Journal:	*Photochemistry and Photobiology*
Manuscript ID	PHP-2018-01-RA-0007.R1
Wiley - Manuscript type:	Research Article
Date Submitted by the Author:	31-Mar-2018
Complete List of Authors:	Barnard, Isla; University of St Andrews, School of Physics and Astronomy Tierney, Patrick; Ninewells Hospital, Photobiology Unit Campbell, Catherine Louise; University of St. Andrews, School of Physics & Astronomy McMillan, Lewis; University of St. Andrews, School of Physics & Astronomy Moseley, Harry Eadie, Ewan; Ninewells Hospital, Photobiology Unit Brown, C; University of St. Andrews, School of Physics & Astronomy Wood, Kenny; University of St. Andrews, School of Physics and Astronomy
Keywords:	UV, UVA, DNA Damage

Quantifying direct DNA damage in the basal layer of skin exposed to UV radiation from sunbeds

Isla Rose Mary Barnard [1], Patrick Tierney [2], Catherine Louise Campbell [2], Lewis McMillan [1], Harry Moseley [2], Ewan Eadie [2], Christian Tom Alcuin Brown [1], Kenneth Wood [1]

[1]. SUPA, School of Physics and Astronomy, University of St Andrews, North Haugh, St Andrews, KY16 9SS, UK, [2]. Photobiology Unit, Ninewells Hospital & Medical School, Dundee, DD1 9SY, UK

*Corresponding author e-mail: irmb@st-andrews.ac.uk (Isla Rose Mary Barnard)

ABSTRACT

Non-melanoma and melanoma skin cancers are attributable to DNA damage caused by ultraviolet (UV) radiation exposure. One DNA photoproduct, the Cyclobutane Pyrimidine Dimer (CPD), is believed to lead to DNA mutations caused by UV radiation. Using radiative transfer simulations, we compare the number of CPDs directly induced by UV irradiation from artificial and natural UV sources (a standard sunbed and the midday summer Mediterranean sun) for skin types I and II on the Fitzpatrick scale. We use Monte Carlo Radiative Transfer (MCRT) modelling to track the progression of UV photons through a multi-layered three dimensional (3D) grid that simulates the upper layers of the skin. By recording the energy deposited in the DNA containing cells of the basal layer, the number of CPDs formed can be quantified. The aim of this work was to compare the number of CPDs formed in the basal layer of the skin, and by implication the risk of developing cancer, as a consequence of irradiation by artificial and natural sources. Our simulations show that the number of CPDs formed per second during sunbed irradiation is almost three times that formed during solar irradiation.

INTRODUCTION

Over-exposure to ultraviolet (UV) radiation is a major cause of skin cancer (1, 2) although the risks from solar UV radiation can be reduced by covering skin, or by using sunscreen (1). One common avoidable source of UV radiation is an artificial tanning unit (hereafter referred to as a sunbed).

Terrestrial UV radiation is classified into the UVA (315 nm to 400 nm) and UVB (280 nm to 315 nm), both of which cause damage to the skin (1).

The processes that lead from UV radiation exposure to skin cancer (photocarcinogenisis) are complex and involve the interplay between various biochemical processes (3). UV radiation reaching cells containing DNA (as illustrated in Figure 1) can damage DNA via several mechanisms. When DNA absorbs UV radiation directly, chemical bonds can be altered, producing DNA photoproducts. These include cyclobutane pyrimidine dimers (CPDs) and pyrimidine (6-4) photoproducts (6-4 PPs). UV radiation can also form reactive oxygen species (ROS) within the cell, which can cause chemical reactions that lead to DNA damage (3). CPDs have been shown to form after exposure to UV has ceased in both melanin rich melanocytes (4) and in keratinocytes containing no melanin (5). These are known as ‘dark CPDs’ and can contribute up to half of the total CPD yield observed in melanocytes (4). The formation of UV-induced DNA photoproducts is very common and on average each skin cell forms 50-100 photoproducts per second of sunlight exposure, though most occurrences are corrected by cell repair processes (6,7). If damage caused by a photoproduct is not corrected, the DNA sequence can be miscopied, leading to a mutation. If this mutation occurs in a gene involved in cancer formation, for example the tumour suppressor gene p53, this may have serious consequences

(2,3). Previously only UVB has been considered to carry sufficient energy to cause damage to cells, however UVA radiation has recently been shown to also be cytotoxic (8,9).

The basal layer of the skin can accumulate enough DNA damage to lead to cancer (10). In healthy skin, the basal layer (Layer 4 in Figure 1) produces skin cells, some of which undergo a process of terminal differentiation, moving upwards, reaching the stratum corneum (Layer 1 in Figure 1) in about 2 weeks. The epidermal layer of skin (Layer 2 in Figure 1) can also acquire DNA damage, however as the cells are committed to terminal differentiation, this is unlikely to have serious consequences (10,11).

The Monte Carlo Radiative Transfer (MCRT) method we apply uses localized probabilities describing photon behavior to model the paths of many photon packets (hereafter referred to as 'power packets') through a scattering and absorbing medium. MCRT is well optimized to model a complex structure such as the skin, as multiple physical quantities can be recorded simultaneously, with desired spatial resolution limited only by the computational power available. Multi-layered 3D MCRT grid codes have been extensively used for various purposes in modelling light-tissue interactions (12-14). By applying MCRT to simulate photon transport through skin tissue, the number of CPDs induced by UV irradiation can be estimated.

The aim of the work presented here is to quantify direct DNA damage in skin types I and II caused by irradiation from a typical UK sunbed in comparison to the damage caused by a high solar UV exposure, chosen as the solar spectrum from a cloudless day in July at midday in Thessaloniki, Greece (15,16). The spectra used are shown in Figure 2. The MCRT codes used are an extension of codes developed by our group for modelling light transport in skin (14,17).

MATERIALS AND METHODS

A 3D grid was built for the MCRT simulation containing optical properties that could be varied on a voxel by voxel basis allowing multiple layer skin structures to be simulated. By tracking the progress of a power packet through the grid, and recording the energy absorbed by the DNA present in the basal layer, the number of CPDs formed could be calculated.

The original FORTRAN 3D grid code used was developed for astronomy applications from a publicly available code (18,19) which was adapted and validated for tissue optics in previous works (14,17).

Geometry: The 3D grid for simulations is a cube of dimensions 1 mm × 1 mm × 1mm and contains 10^6 cubic voxels of side 0.01 mm. Within a single voxel the optical properties are homogeneous. Each voxel is allocated specific optical properties depending upon its spatial location, allowing the structure of skin to be simulated via the five-layer model shown in Figure 1.

>Figure 1<

In the model, the top layer of the skin, the stratum corneum (layer 1), has a flat surface and base. Below this is the epidermal layer (layer 2) which has an undulating shape to represent the dermal papillae. Layer 3 is a layer of melanised epidermis which, in non-UV adapted skin types I-II takes the form of melanosomes residing above the basal layer (layer 4) (20, 21). This model simulates skin types I-II by concentrating the melanin fraction above the basal layer (layer 4). Skin types III-VI are not represented by this model; as in these skin types melanin is distributed throughout the epidermis in varying concentrations. The final layer in this model (layer 5) is the dermis.

The maximum and minimum depth of each layer from the surface are shown in Figure 1, and the average depth from the surface is shown in Table 1. The base of the stratum corneum (layer 1) is considered to be flat, along with the base of the modelled dermis (layer 5) which marks the bottom of the 3D grid. The base of the epidermis (layer 2), melanin layer (layer 3), and basal layer (layer

4) are modeled using a 3D sinusoid to approximate the shape of dermal papillae (Equation 1) where z(x,y) is the surface of the layer in mm, x and y are the horizontal coordinates, and the depth is the average depth of each layer from the surface as listed in Table 1.

$$z(x,y) = 0.03mm \times \sin(x/0.015mm) \times \sin y/(0.015mm) + depth \qquad (1)$$

>Table 1<

To simulate a layer of skin, repeating boundaries were implemented on the vertically oriented faces of the grid. A power packet leaving the grid on a vertical face rejoins the grid on the opposing vertical face; with all properties pertaining to the power packet other than position retained. This simulates an infinitely repeating medium in the horizontal directions, and so approximates a 1mm^2 section of a large area of skin of depth 1 mm.

Irradiation: MCRT works by simulating the progress of one power packet at a time through the medium. A power packet is initialized with a spatial location in the grid, an initial direction of travel, and a single wavelength. To simulate irradiation from a broadband source, a wavelength is obtained using a random sampling of the spectral irradiance of the source spectrum.

To quantify the DNA damage caused by a typical UK sunbed, a suitable UV source was chosen. The sunbed spectrum was typical of those measured in a recent study that also found that over 90% of such devices exceeded the maximum effective irradiance recommended by the European Commission (23,24). A spectrum from Thessaloniki in Greece in midsummer at midday gives an example of a natural environment with high UV exposure (15,16). The spectra used in our simulations are shown in Figure 2.

>Figure 2<

The sunbed was considered a purely diffuse source, and the solar spectrum a mix of direct and diffuse components determined by the latitude and longitude of the location on earth where the spectrum was recorded (25). In this model, direct components are modelled as power packets with a direction of entry normal to the surface of the grid, and diffuse components are modelled by assigning a random direction of entry to the grid. For both sources, the initial position of the power packet is randomly sampled to simulate uniform irradiation of the surface.

Due to the refractive index change between the air and the surface of the skin, Fresnel reflections are taken into account at this boundary. Power packets leaving the simulated skin structure at the lower face are terminated. Fresnel reflections between the layers within the skin are not accounted for.

Absorption and Scattering: The path taken by a photon through the simulated tissue structure is determined by the optical properties assigned to each voxel, comprising the absorption and scattering coefficients μ_a and μ_s , the refractive index n, and the scattering anisotropy factor g assigned to individual voxels. In general, there is a high level of variability of optical properties between individuals and from published literature (26, 27).

The upper epidermal layers (layers 1, 2 and 3 in Figure 1) residing above the basal layer are responsible for the majority of the attenuation of UV radiation reaching the basal layer. UV radiation reaching the dermis is also scattered back to the basal layer; as there is no protective melanin at the basal-dermal junction this represents an important component of the model.

The Henyey Greenstein phase function, $HG(\theta)$ used throughout the model is described by Equation 2 and is used in conjunction with the anisotropy factor g (defined as the average of

143 $\cos\theta$ where θ is the angle between the direction of travel and the direction of scattering, described
144 by Equation 3) to model the angular scattering phase function, as skin is highly forward scattering
145 (28, 29). The anisotropy factor g is wavelength dependent and is described by Equation 4
146 throughout the model, where the wavelength λ is given in nm. In Equation 2, θ is the scattering
147 angle and g is the anisotropy factor $-1 \leq g \leq 1$.
148

$$HG(\theta) = \frac{1}{4\pi(1 + g^2(\lambda) - 2g(\lambda)\cos\theta)^{\frac{3}{2}}} \quad (2)$$

$$g(\lambda) = \langle\cos\theta\rangle = \int_0^{\pi} HG(\theta)\cos\theta\, 2\pi\sin\theta\, d\theta \quad (3)$$

$$g(\lambda) = 0.62 + 0.29\lambda \times 10^{-3} \quad (4)$$

149
150 Within our work, the g values vary linearly between 0.7 and 0.74 as described by Equation 4 and
151 the refractive index of tissue $n = 1.38$.
152 The optical properties used to characterize the stratum corneum and the epidermal layers are from
153 data published by Van Gemert et al. (29) who derived absorption and scattering spectra by
154 transforming experimentally determined transmittance and reflectance spectra.
155 The stratum corneum provides significant protection against UV radiation, due to the strong
156 preference for absorption and scattering in the UVB; although absorption and scattering is high
157 throughout the full UV spectrum. It is assumed the stratum corneum contains no melanin in skin
158 types I and II, and as such the skin type has no influence on the absorption or scattering properties.
159 The wavelength dependent absorption for the stratum corneum is shown in Figure 3; and the
160 wavelength dependent scattering spectrum is shown in Figure 4.
161 >Figure 3<

>Figure 4<

The epidermis is the layer of the skin above the basal layer, and as such, the scattering and absorption of UV radiation within the epidermis has a significant effect on the amount of UV radiation absorbed by the basal layer. The epidermal layer also contains living cells that are susceptible to UV induced DNA damage. The properties used to model this layer are from the properties published by Van Gemert et al. (29). The original experimental data were measured using 'medium complexioned Caucasian skin' and the epidermal absorption coefficients reported describe all the sum total of absorption coefficients due to all chromophores present in skin tissue. Using melanin concentrations described by Karsten et al. (20), it was assumed the experimental data described skin with a melanin volume fraction V_{mel} of 4 % (33, 34). This contribution is removed from the epidermal layer (layer 2) to simulate epidermis without melanin; as shown in Figure 3. The skin type dependent contribution of melanin to the absorption of the epidermis is calculated and concentrated in the melanin layer (layer 3).

Melanin is the primary chromophore responsible for shielding the DNA-containing basal layer from DNA damage (35). The estimated volume fraction of melanin present in the skin V_{mel} is skin type dependent, and ranges from 0-3% for skin type I, and from 3-5% for skin type II (20, 21, 36). Values of 2% for skin type I and 4% for skin type II were chosen. In the skin, melanin is created by melanocytes in the form of melanosomes, and is present in two types (eumelanin is a brown or black pigment, and pheomelanin is a red pigment). Melanosomes are taken up by keratinocytes, where they cluster around the nucleus, shielding DNA. To simulate this distribution of melanin, a single layer of melanin is modelled above the basal layer, shown in Figure 1. To model the optical properties for skin types I-II, the absorption resulting from the melanin volume fraction

corresponding to the skin type was added to the epidermal optical properties; as shown in Figure 3. The optical properties resulting from a combination Eumelanin and pheomelanin are modelled using Equation 5 (32), where the wavelength λ is given in nm, $V_{mel}$is the volume fraction of melanin in the tissue, and the absorption coefficient $\mu_{a,mel}$ is given in cm^{-1}.

$$\mu_{a,mel}(\lambda) = 6.6 \times 10^{11}\lambda^{-3.33}V_{mel} \qquad (5)$$

In the model, the contribution of melanin to the epidermal layer absorption coefficient is removed from layer 2 and concentrated in a single layer of voxels (layer 3) sited directly above the DNA containing basal layer (layer 4). These absorption coefficients are shown in Figure 3. The scattering coefficient μ_s (given in cm^{-1}) for the epidermal and melanin layers are considered to exhibit the same wavelength dependence, as shown in Figure 4.

The epidermal layer and the basal layer both contain DNA. DNA is a strong absorber of UVB radiation, as indicated in Figure 3. The extinction coefficient spectrum of oligomeric duplex dA20:dT20 has previously been used to determine photo-damage in DNA (31) and is used here as an approximation for the absorption coefficient of the DNA contained within cells. The concentration of DNA within the epidermal and basal layers is estimated using a volumetric method adapted from Mohlenhoff et al (30). Using the number of bases per human diploid cell (12.8 billion bases) along with average cell sizes for cells in the basal layer and epidermis (on average 13 µm and 20 µm respectively (37)), cells in the epidermal layers (layers 2 & 3) are estimated to have a DNA concentration of approximately 0.005 moles per liter, and those in the basal layer to have a DNA concentration of 0.018 moles per liter.

Equation 6 is used to combine these concentrations with the extinction coefficient per base taken

from Mouret et al. (31) to retrieve the absorption coefficient $\mu_{a,DNA}$ (where the wavelength λ is given in nm and $\mu_{a,DNA}$ is given in cm^{-1}). The DNA absorption is shown in Figure 3 for layers 2, 3 and 4. The scattering in the basal layer (layer 4) is considered to follow the wavelength dependent form described by Equation 7 (32), where λ is given in nm and μ_s is given in cm^{-1}.

$$\mu_{a,DNA}(\lambda) = \log_e(10)\,\epsilon_{DNA}(\lambda) C_{DNA} \qquad (6)$$

$$\mu_s(\lambda) = 1.752 \times 10^8\,\lambda^{-2.33} + 134.67\lambda^{-0.494} \qquad (7)$$

The Dermis is the deepest layer of skin included in our model. Equation 8 (32) describes $\mu_{a,dermis}$ (where $\mu_{a,dermis}$ is given in cm^{-1} and the wavelength λ is given in nm).

$$\mu_{a,dermis}(\lambda) = (1 - f_{blood})\mu_{base}(\lambda) + f_{blood}\,\mu_{a,blood}(\lambda) \qquad (8)$$

$$\mu_{a,blood}(\lambda) = \frac{1}{\omega_{hgb}} \log_e(10)\left(\epsilon_{a,ohb}(\lambda) SO_2 + \epsilon_{a,dhb}(\lambda)(1 - SO_2)\right) C_{hb} \qquad (9)$$

$$\mu_{base}(\lambda) = 7.84 \times 10^7 \times \lambda(nm)^{-3.255} \qquad (10)$$

To determine the absorption coefficient for blood $\mu_{a,blood}(\lambda)$ as used in Equation 8, Equation 9 is used. The hemoglobin concentration C_{hb} of 150 gL^{-1} and an oxygen saturation SO_2 of 75 % are used in Equation 9 (where λ is given in nm); and the extinction coefficients for hemoglobin are taken from Jacques et al. (32). The molecular weight of hemoglobin ω_{hgb} is 64458g/mol. The background absorption, $\mu_{base}(\lambda)$ is taken from Jacques et al. (32).

The absorption coefficient $\mu_{a,blood}(\lambda)$, is shown in Figure 3. The scattering coefficient is equivalent to that described for the basal layer by Equation 7 and shown in Figure 4.

The MCRT model allows recovery of the number of absorbed photons and the wavelength dependent fluence rate in all the voxels in the model. Using this, the number of photons absorbed by the basal layer can be determined. For a photobiological process, such as CPD formation, the efficiency may be described by the quantum yield, ϕ, expressed as

$$\phi = \frac{N_{process}}{N_{absorbed}} \qquad (11)$$

Where $N_{process}$ is the number of photons causing the biological effect and $N_{absorbed}$ is the total number of absorbed photons. Banyasz et al. demonstrated quantum yields for CPD formation to be 0.05 for UVB and 0.0005 for UVA (38). The number of absorbed photons for sunlight and sunbed sources were evaluated and compared. To attempt to quantify the additional risk to human health of sunbed use, CPDs and photons absorbed due to sunbed irradiation are expressed as a proportion of those absorbed due to solar irradiation, as risks to health from solar irradiation are well characterized (15).

RESULTS

Figure 5 shows maps detailing the total number of absorbed photons per second through a central slice of the 3D grid for both the Mediterranean sun and the sunbed for skin type I and skin type II. The maps clearly show the high absorption by melanin residing above the basal layer; and that more photons are absorbed by the grid simulating sunbed irradiation. Spotting at the base of the grids is characteristic Monte Carlo noise. A running total for energy absorbed by each voxel in the grid as a function of wavelength is recorded throughout the simulation. In

the map presented in Figure 5, the total number of photons is presented (obtained using Equation 12, and summing over all wavelengths), and no wavelength dependent information remains.

$$N_\lambda = \frac{E_{\lambda,voxel}}{E_{\lambda,photon}} = \frac{\lambda E_{\lambda,voxel}}{hc} \qquad (12)$$

>Figure 5 <

Table 2 presents results obtained when the depth of the epidermal layer is varied, showing as the depth of the epidermis is increased, the ratio of CPDs formed within the basal layer increases, while the total ratio of photons absorbed decreases. The wavelength dependent energy absorbed within the basal layer was isolated, and using the quantum yields for CPD formation of 0.05 for UVB and 0.0005 for UVA (38) with Equation 11, the number of CPDs formed is retrieved. The number of CPDs formed by the sunbed is expressed as a fraction of those formed by the Medditeranean sun.

>Table 2<

An example of the proportions of CPDs formed within the basal layer with respect to skin type and UV band is shown in Table 3. The number of CPDs formed by the sunbed is expressed as a fraction of those formed by the Medditeranean sun.

>Table 3<

Figure 6 shows the fluence incident on the basal layer for both skin types and both radiation sources. Throughout the simulation, the fluence incident on each voxel is recorded for the

whole grid. The fluence incident on the voxels corresponding to the basal layer is extracted and shown in Figure 6.

>Figure 6<

CPDs are not just formed in the basal layer of the skin, as cells in the epidermis (layers 2 & 3 in Figure 1) also contain DNA. The numbers of CPDs formed per $1mm^2$ skin comprising epidermis and basal layer is presented in Table 4.

>Table 4<

DISCUSSION

Previous work suggests that 90 % of sunbeds in the UK emit UV levels exceeding current EU recommended limits (23). On-site sunbed measurements were used to evaluate exposure scenarios. Further study quantified the increased risk in developing squamous cell carcinoma by age 55 years in terms of additional doses of UV radiation due to sunbed use between the ages of 20-35 years. The lowest 5^{th} percentile of additional UV exposure (corresponding to 83 standard erythemal doses) increased the risk of developing squamous cell carcinoma by 40 %. At the 95^{th} percentile of additional exposure (corresponding to 302 standard erythemal doses) the risk had increased by 300 % (15).

In the present study, MCRT modelling was used to simulate the transmission of UV radiation through the upper layers of skin tissue. We used published optical properties in a five-layer model comprising the stratum corneum, non melanised epidermis, a melanin layer, the basal layer (in which skin stem cells reside) and the dermis. The basal layer and the protective

284 melanin were modelled with a 3D sinusoidal surface as an approximation to the undulating
285 shape of the dermal papillae folds.

286 MCRT modeling to simulate UV transport through skin tissue allows complete control over
287 parameters such as the optical properties; in contrast to laboratory experiments where optical
288 properties would likely vary within and across individuals. MCRT also allows wavelength
289 dependent results to be extracted from selected tissue depths irradiated with real-world
290 sources, such as the sun, without attempting to simulate such wavelength dependence with a
291 monochromator. A model of this type is currently unable to fully simulate the many pathways
292 by which UV radiation causes damage to skin. CPDs are often found within signature
293 mutations in UV induced non melanoma skin cancers (SCCs and BCCs) that are linked to
294 lifetime cumulative UV exposure (15), and as such the CPD yield was chosen as an indicator
295 for DNA damage. However the model does not include UV induced enzymatic DNA repair
296 mechanisms (which would reduce the total number of CPDs formed), nor other sources of
297 CPD formation, such as those formed by ROS initiated by UV absorption (3), or dark CPDs
298 formed both with and in the absence of melanin (4,5). As a result, the model is likely to
299 underrepresent the total number of CPDs formed and by way of compensation, ratios of
300 sunbed induced CPDs to solar induced CPDs are presented. It may be possible to extend the
301 model to take these processes into account by adding a time dependent aspect to the model
302 following initial irradiation, allowing repair processes to be modelled along with dark CPDs.

303 This model is only applicable to Fitzpatrick skin types I-II that are not UV adapted, where the
304 melanin resides immediately above the basal layer; however the model could be adapted to
305 simulate other skin types. As part of the response to UV radiation, melanin moves up into the
306 epidermal layer and more melanin is created by melanosomes in the basal layer (35); although

research indicates that the role of melanin can no longer be considered as purely protective, and it may in fact be carcinogenic (4). When skin is not UV adapted, the UV radiation causes greater risk to skin health due to the lower concentration of melanin in the epidermis. However what we have done is to quantify, for the first time, the relative risk of direct CPD formation from sunbed use compared to solar exposure. By implication this quantifies the risk of direct DNA damage due to exposure to UV radiation from a sunbed in comparison to that from Mediterranean sunlight.

By utilizing the optical properties for DNA and the quantum yield for CPDs the number of CPDs formed was calculated. The simulation was run with a typical sunbed spectral irradiance and, for comparison, solar irradiance. Both sunbeds and sunlight are primarily UVA sources; and direct CPDs are primarily formed by UVB; indicating that true CPD yields, including those due to ROS and dark CPDs (4,5) are likely to be higher than those stated here. Table 4 details for skin type I that for solar irradiation, UVB radiation results in a higher proportion of CPDs formed in the basal layer than for UVA radiation, even though only 0.5 % of UVR radiation incident on the basal layer is UVB (Figure 6). However, for sunbed irradiation, UVA radiation is responsible for the majority of CPDs formed in the basal layer. This is an important finding, as it shows that even though the yield for UVA CPDs is 100 times less than that for UVB (38), the high UVA output of the sunbed results in the majority of CPDs being formed due to UVA radiation.

Table 4 also details the total number of CPDs formed in the epidermis for the skin type I sample. For solar and sunbed UVA irradiation, there are about 4.6 times more CPDs formed in the epidermis than in the basal layer respectively. For solar and sunbed UVB radiation, there are about 7 times more CPDs formed in the epidermis than in the basal layer. Although the

DNA concentration in the basal layer is approximately 4 times higher than that in the epidermis; there are 8 times as many voxels comprising the epidermis than comprising the basal layer. This, coupled with the fact that the epidermis is closer to the surface, and the small penetration depth of UVB coupled with the high UVB CPD yield explains why so many more CPDs are formed in the epidermis than in the basal layer. As keratinocytes in the epidermis are likely to be committed to terminal differentiation, any damage accumulated here is unlikely to have long term consequences (10, 11). As a result, it may be that DNA within the epidermis actually plays a protective role in shielding the basal layer from UV radiation.

Figure 6 shows the fluence incident on the basal layer for both skin types and both irradiation sources. In both cases, radiation below 315nm (UVB), reaches the basal layer although in small amounts. UVB is strongly absorbed by DNA (30) and UVB CPDs have a high quantum yield (31). The basal layer has a high concentration of DNA (37) and is considered the layer of the skin that can accumulate enough DNA damage to cause risk to human health (10). The argument that UVB radiation can not penetrate far enough into the epidermis to cause significant damage to the basal layer is not supported by this model. However, it is important to note that for solar radiation, the incident radiation contains 3 % UVB, and for the sunbed, the incident radiation contains 1.4 % UVB (see Figure 2). For both sunbed and solar irradiation, of the total fluence incident on the basal layer, the percentage of UVB radiation is greatly reduced from that incident on the skin surface (see Figure 6) This is due to the shielding effects of the upper layers of the epidermis, and the wavelength dependent absorption by the upper layers of skin.

Absolute numbers of CPDs formed in the basal layer differ between the skin types, as shown in Figure 5, Table 4, and indicated by the difference in fluence rate in the basal layer (see

Figure 6). However, if the risk of DNA damage from sunbed use for one skin type can be deduced from the ratio between the number of CPDs formed due to sunbed exposure to the number formed due to solar exposure, then Table 3 indicates that for both skin types, the additional risk is almost equal; despite skin type II containing twice as much melanin (20,21).

Increasing the depth of the epidermal layer appears to gradually increase the ratio between sunbed and solar CPD formation, despite the ratio of photons absorbed decreasing. This is due to UVA penetrating deeper than UVB; and continuing to produce CPDs. This indicates that UVA radiation may also affect live cells residing in layers of the skin deeper than the basal layer.

Conclusion

When skin is irradiated with a sunbed, UVA photons make a large contribution to CPD formation. For both sources, UVA radiation contributes significantly to the total amount of CPDs formed. This is despite UVB being preferentially absorbed by DNA compared to UVA, and also forming more CPDs per absorbed UVB photon than per absorbed UVA photon, and despite UVB being generally considered to be the part of the UV spectrum to present the greater risk to human health. We estimate that for skin type I, 12 min on a typical sunbed produces approximately the same amount of DNA damage as 30 min sunbathing in the midday Mediterranean summer sun. We present similar results for CPD formation ratios for both skin types, indicating that the relative increase in DNA damage from sunbed use may be the same for both skin types I and II.

ACKNOWLEDGMENTS: Isla Rose Mary Barnard acknowledges financial support from an UK EPRSC PhD studentship EP/N509759/1.

SUPPLEMENTARY MATERIALS

REFERENCES

1. Narayanan, D. L., R. Saladi and J. Fox (2010) Ultraviolet radiation and skin cancer. Int J Dermatol. 49, 978–86.

2. Leiter, U. and C. Garbe (2008) Epidemiology of melanoma and non melanoma skin cancer- the role of sunlight. Adv Exp Med Biol. 624, 89-103.

3. Black, H. S. and F. deGruijl (1997) Photocarcinogenesis: an overview. J Photochem Photobio B. 40, 29–47.

4. Premi, S., S. Wallisch, C. M. Mano, A. B. Weiner, A. Bacchiocchi, K. Wakamatsu, and D. E. Brash (2015) Chemiexcitation of melanin derivatives induces DNA photoproducts long after UV exposure. Science. 347(6224), 842-847.

5. Delinasios, G. J., M. Karbaschi, M. S. Cooke and A. R. Young (2018) Vitamin E inhibits the UVAI induction of "light" and "dark" cyclobutane pyrimidine dimers, and oxidatively generated DNA damage, in keratinocytes. Sci Rep. *8*(1), 423.

6. Goodsell, D. S. (2001) The molecular perspective: ultraviolet light and pyrimidine dimers. The Oncologist. 6(3), 298-299.

7. Lindahl, T. and R. D. Wood (1999) Quality control by DNA repair. Science. 286(5446), 1897-1905.

8. Huang, X. X., F. Bernerd and G. M. Halliday (2009) Ultraviolet A within sunlight induces mutations in the epidermal basal layer of engineered human skin. Am J Pathol. 174(4), 1534-1543.

9. Boniol, M., P. Autier, P. Boyle and S. Gandini (2012) Cutaneous melanoma attributable to sunbed use: systematic review and meta-analysis. BMJ. 345, e4757.

10. Owens D. M., and F. M. Watt (2003) Contribution of stem cells and differentiated cells to epidermal tumors. Nat Rev Cancer. 3, 444-451.

11. Young, A. R., G. I. Harrison, C. A. Chadwick, O. Nikaido, J. Ramsden, and C. S. Potten (1998) The similarity of action spectra for thymine dimers in human epidermis and erythema suggests that DNA is the chromophore for erythema. J Invest Dermatol. 111(6), 982-988.

12. Wang, L., S. L. Jacques and L. Zheng (1995) MCML—Monte Carlo modeling of light transport in multi-layered tissues. Comput Methods Programs Biomed. 47(2), 131-146.

13. Boas, D. A., J. P. Culver, J. J. Stott and A. K. Dunn (2002) Three dimensional Monte Carlo code for photon migration through complex heterogeneous media including the adult human head. Opt express. 10(3), 159-170.

14. Campbell, C. L., C. Christison, C. T. A. Brown, K. Wood, R. M. Valentine and H. Moseley (2015) 3D Monte Carlo radiation transfer modelling of photodynamic therapy. Proc SPIE. 9531(Biophotonics South America).

15. Tierney, P., F. R. Gruijl, S. Ibbotson and H. Moseley (2015) Predicted increased risk of squamous cell carcinoma induction associated with sunbed exposure habits. Br J Dermatol. 173(1), 201-208.

16. Zempila M., J. H. G. M. van Geffen, M. Taylor, I. Fountoulakis, M. Koukouli, M. van Weele, R. J. van der A, A. Bais, C. Meleti and D. Balis (2017) TEMIS UV product validation using NILU-UV ground-based measurements in Thessaloniki, Greece. Atmos Chem Phys, 17, 7157-7174.

17. Campbell, C. L., K. Wood, R. M. Valentine, C. T. A. Brown and H. Moseley (2015) Monte Carlo modelling of daylight activated photodynamic therapy. Phys Med Biol. 60(10), 4059.

18. Wood, K. and R. J. Reynolds (1999) A model for the scattered light contribution and polarization of the diffuse Hα galactic background. ApJ. 525(2), 799.

19. Wood, K., L. M. Haffner, R. J. Reynolds, J. S. Mathis and G. Madsen (2005) Estimating the porosity of the interstellar medium from three-dimensional photoionization modeling of Hii regions. ApJ. 633(1), 295

20. Karsten, A. E., and J. E. Smit (2012). Modeling and verification of melanin concentration on human skin type. Photochem Photobiol. 88(2), 469-474.

21. Fitzpatrick, T. B. (1988) The validity and practicality of sun-reactive skin types I through VI. Arch Dermatol. 124(6), 869-871.

22. Lock-Andersen, J., P. Therkildsen, F. Olivarius, M. Gniadecka, K. Dahlstrem, T. Poulsen, and H. C. Wulf (1997) Epidermal thickness, skin pigmentation and

constitutive photosensitivity. Photodermatol Photoimmunol Photomed. 13(4), 153-158

23. Tierney, P., J. Ferguson, S. Ibbotson, R. Dawe, E. Eadie and H. Moseley (2013) Nine out of 10 sunbeds in England emit ultraviolet radiation levels that exceed current safety limits. Br J Dermatol. 168(3), 602-608.

24. European commission scientific committee on consumer products (2006) Preliminary opinion on biological effects of ultraviolet radiation relevant to health with particular reference to sun beds for cosmetic purposes. European Commission.

25. Bird, R. E. (1984) A simple, solar spectral model for direct-normal and diffuse horizontal irradiance. Solar energy. 32(4), 461-471.

26. Lister, T., P. A. Wright and P. H. Chappell (2012) Optical properties of human skin. J Biomed Opt. 17(9), 0909011-09090115.

27. Jacques, S. L. (2013). Optical properties of biological tissues: a review. Phys Med Biol. 58(11), R37.

28. Bruls, W. A. and J. C. Van Der Leun (1984) Forward scattering properties of human epidermal layers. Photochem Photobiol. 40(2), 231-242.

29. Van Gemert, M. J., S. L. Jacques, H. J. Sterenborg and W. M. Star (1989) Skin optics. IEEE Trans Biomed Eng. 36(12), 1146-1154.

30. Mohlenhoff, B., M. Romeo, M. Diem and B. R. Wood (2005) Mie-type scattering and non-Beer-Lambert absorption behavior of human cells in infrared microspectroscopy. Biophys J, 88(5), 3635-3640.

31. Mouret, S., C. Philippe, J. Gracia-Chantegrel, A. Banyasz, S. Karpati, D. Markovitsi and T. Douki (2010) UVA-induced cyclobutane pyrimidine dimers in DNA: a direct photochemical mechanism? Org Biomol Chem. 8(7), 1706-1711.

32. Jacques, S. L. (1998) Skin optics. Oregon Medical Laser Center News 1998. 1, 1-9.

33. Wan, S., R. Anderson and J. A. Parrish (1981) Analytical modeling for the optical properties of the skin with in vitro and in vivo applications. Photochem Photobiol. 34(4), 493-499.

34. Everett, M. A., E. Yeargers, R. M. Sayre and R. L. Olson (1966) Penetration of epidermis by ultraviolet rays. Photochem Photobiol. 5(7), 533-542.

35. Brenner, M., and V. J. Hearing (2008). The protective role of melanin against UV damage in human skin. Photochemistry and photobiology, 84(3), 539-549

36. Iglesias-Guitian, J. A., C. Aliaga, A. Jarabo and D. Gutierrez (2015) A biophysically-based model of the optical properties of skin aging. Computer Graphics Forum. 34(2), 45-55.

37. Watt, F. M., and H. Green (1981) Involucrin synthesis is correlated with cell size in human epidermal cultures. J Cell Bio. 90(3), 738-742.

38. Banyasz, A., T. Douki, R. Improta, T. Gustavsson, D. Onidas, I. Vayá and D. Markovitsi (2012) Electronic excited states responsible for dimer formation upon UV absorption directly by thymine strands: joint experimental and theoretical study. J Am Chem Soc. 134(36), 14834-14845.

TABLES

Layer Number	Skin Layer	Average Depth from Surface (mm)
1	Stratum Corneum	0.02
2	Epidermis	0.08
3	Melanin Layer	0.09
4	Basal Layer (DNA Layer)	0.10
5	Dermis	(base of grid)

476 **Table 1**. Average depth of each layer from the surface of the 3D grid taken from Lock-
477 Anderson et al (22). Layer 1 (stratum corneum) and Layer 5 (dermis) both have flat bases. The
478 average depths listed for the epidermis (layer 2), the melanin layer (layer 3) and the basal layer
479 (layer 4) are added to Equation 1 to model the shape shown in Figure 1.

480

Epidermis/Basal/Dermis Depths (μm)	Photons Absorbed $^{Sunbed}/_{Solar}$	CPDs $^{Sunbed}/_{Solar}$
70/80/90	4.17	2.48
80/90/100	4.16	2.50
90/100/110	4.15	2.65
100/110/120	4.16	2.74
110/120/130	4.15	2.75

481 **Table 2**. Ratios of photons absorbed between sunbed and solar irradiation, and CPDs created,
482 for skin type I with varying epidermal depths, to approximate sites on the body of varying
483 epidermal depths. The 20 μm depth of the stratum corneum is maintained, as is the 10 μm
484 separation between the epidermal, melanin and basal layers (layers 2, 3 and 4), and the depth
485 of the epidermis is varied from 70 μm to 110 μm. The ratio of CPDs formed is always smaller

than the ratio of absorbed photons. This is due to the strong UVA irradiance from the sunbed, which has a much smaller quantum yield for CPDs.

UV Band	Skin Type I CPDs $^{Sunbed}/_{Solar}$	Skin Type II CPDs $^{Sunbed}/_{Solar}$
UVA	4.21	4.16
UVB	1.68	1.67

Table 3. Proportion of CPDs formed with respect to the band of the UV spectrum examined for skin types I and II. The geometry used is as described in Figure 1, with average depths of 80 μm for the epidermis, 90 μm for the DNA layer and 100 μm for the dermis. Little variation is observed between skin types in the ratios of sunbed to solar UVB induced CPDs, however there is a more marked difference in the ratios of sunbed to solar UVA induced CPDs.

UV Band	CPDs per second per mm^2 (Solar)		CPDs per second per mm^2 (Sunbed)	
	Basal Layer	Epidermis	Basal Layer	Epidermis
UVA	2.41×10^7	1.10×10^8	1.01×10^8	4.76×10^8
UVB	5.01×10^7	3.52×10^8	8.43×10^7	6.12×10^9

Table 4. Absolute numbers of CPDs formed with respect to the band of the UV spectrum and skin layer for skin type II. The geometry used is as described in Figure 1, with average depths of 80 μm for the epidermis, 90 μm for the DNA layer and 100 μm for the dermis. There are 10304 voxels in the basal layer (layer 4), and 61976 voxels in the epidermal layers (layers 2 and 3).

500 **FIGURE CAPTIONS**

501 **Figure 1**. The five-layer skin model used in the simulation; comprising the stratum corneum
502 (layer 1), the epidermis (layer 2), melanin-containing epidermis (layer 3), the basal layer (layer
503 4) and the dermis (layer 5). The figure shows the characteristic egg box sinusoidal pattern as
504 described by Equation 1, which is used to simulate dermal papillae. The inset summarizes the
505 maximum and minimum layer separations chosen to represent the geometry of the skin layers
506 modelled. For color, please see online version.

507 **Figure 2.** Spectra used to simulate irradiation of the skin. In (a) the broken line shows the
508 UV spectrum from a typical sunbed (where the spikes indicate characteristic mercury emission
509 lines) and the solid line shows a solar spectrum, shown alone in inset (b). This spectrum is
510 taken from a cloudless day in July at midday from Thessaloniki in Greece using ground based
511 instrumentation (15,16). UVB radiation is defined as 280 nm to 315 nm and UVA radiation as
512 315 nm to 400 nm. The solar spectrum has a total irradiance of 50.5 Wm^{-2} with a UVB
513 irradiance of 1.5 Wm^{-2} and a UVA irradiance of 49.0 Wm^{-2}. The sunbed spectrum has a total
514 irradiance of 283.0 Wm^{-2} with a UVB irradiance of 4.0 Wm^{-2} and a UVA irradiance of 279.0
515 Wm^{-2}.

516 **Figure 3.** Modelled absorption coefficients as a function of wavelength (nm) as described in
517 the text for the five layer skin model, comprising a) the stratum corneum (layer 1), taken
518 directly from Van Gemert et al. (29) b) epidermis with melanin removed (layer 2), and
519 melanin layer (layer 3), derived using Equation 5 and data from Van Gemert et al. (29), c)
520 DNA absorption coefficients for layers 2,3 and 4 derived using the method described by

Molenhoff et al. (30) and data from Mouret et al. (31) and d) the dermis, using Equations 8 and 9, as described by Jacques et al. (32).

Figure 4. Scattering coefficients as a function of wavelength (nm) of a) the stratum corneum (layer 1), taken directly from Van Gemert et al. (29) and b) the epidermal and melanin layer (layers 2 and 3), taken directly from (29) and the basal and dermal layers (layers 3 and 4) as described by Equation 7 derived by Jacques et al. (32).

Figure 5. Maps of photons deposited in the central slice of the model in terms of number of absorbed photons per cm^3 per second for both skin types. The top of each map shows a bright flat layer, indicating strong absorption in the stratum corneum (layer 1). The bright sinusoidal layer indicates high absorption of UVR in the melanin layer (layer 3), below which darker spots indicate a lower overall level of absorption in the basal layer (layer 4). Dark spotting at the base of layer 5 (the dermis) is characteristic Monte Carlo noise. For color, please see online version.

Figure 6. Radiation incident on the basal layer for a) the solar simulation and b) the sunbed simulation. In both skin types, and for both sources, a small amount of UVB radiation penetrates as far as the basal layer. For a), in skin type I, 99.4 % of fluence reaching the basal layer is UVA, and 0.6 % is UVB. For skin type II, 99.5 % of solar fluence reaching the basal layer is UVA, and 0.5 % is UVB. For b) in both skin types I and II, 99.7 % of fluence reaching the basal layer is UVA, and 0.3 % is UVB. Figure 2 shows the incident solar radiation contains 97 % UVA and 3 % UVB, and the incident sunbed radiation contains 98.6 % UVA and 1.4 % UVB.

543

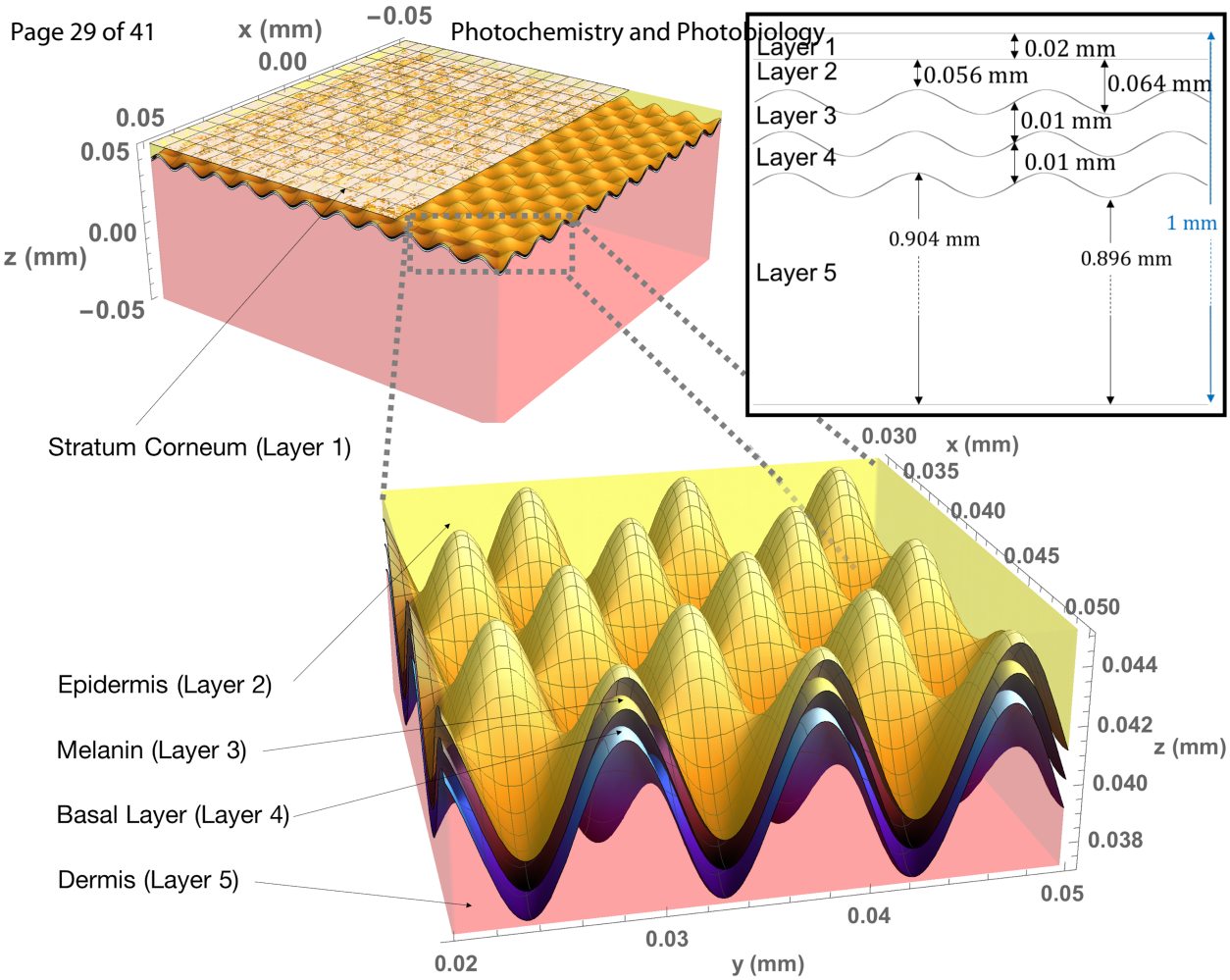
x (mm)
−0.05
0.00
0.05
0.05
0.00
z (mm)
−0.05
Layer 1
Layer 2
Layer 3
Layer 4
Layer 5
0.02 mm
0.056 mm
0.064 mm
0.01 mm
0.01 mm
1 mm
0.904 mm
0.896 mm
Stratum Corneum (Layer 1)
Epidermis (Layer 2)
Melanin (Layer 3)
Basal Layer (Layer 4)
Dermis (Layer 5)
0.030
x (mm)
0.035
0.040
0.045
0.050
0.044
0.042
z (mm)
0.040
0.038
0.02
0.03
0.04
0.05
y (mm)

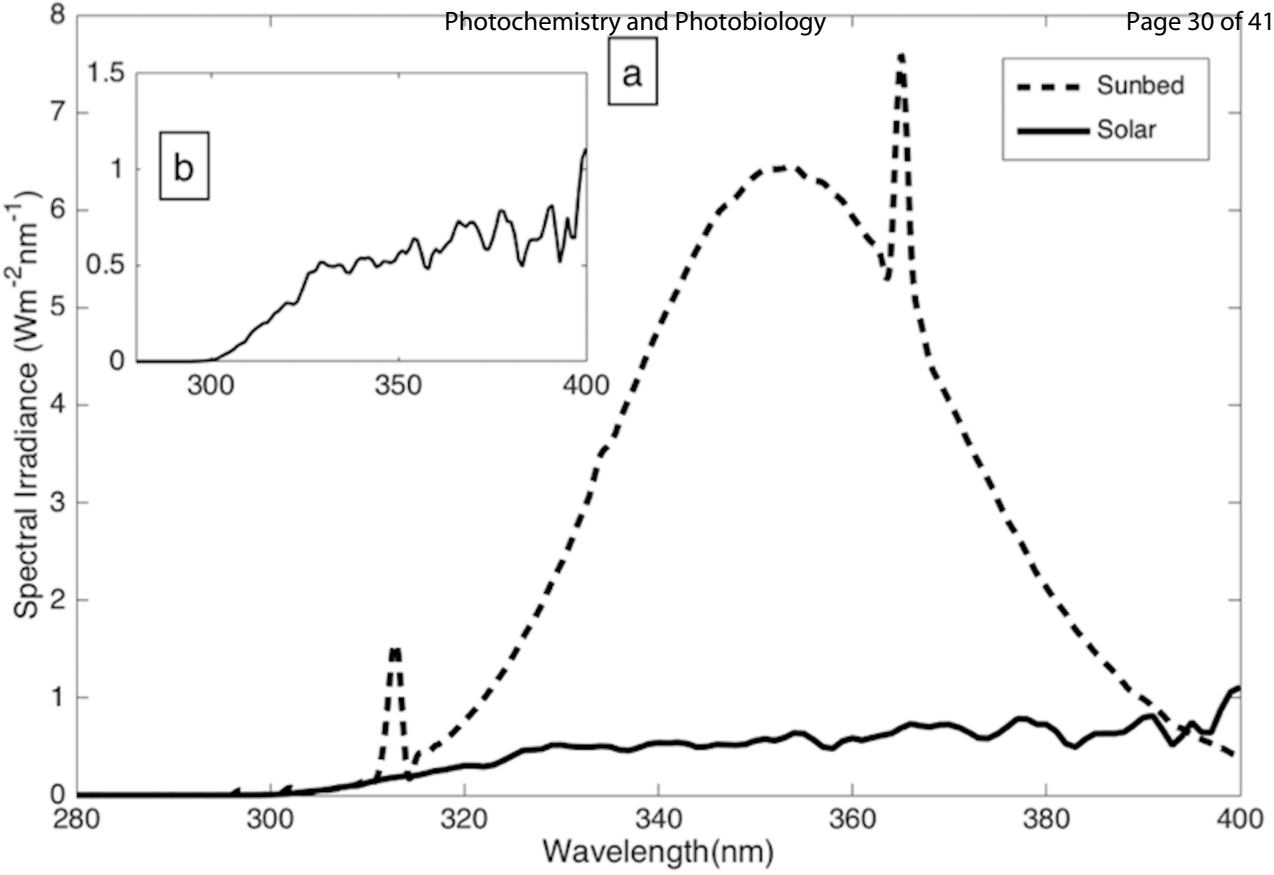
a
b
Sunbed
Solar
Spectral Irradiance (Wm-2nm-1)
Wavelength(nm)
0
1
2
3
4
5
6
7
8
280
300
320
340
360
380
400
0
0.5
1
1.5
300
350
400

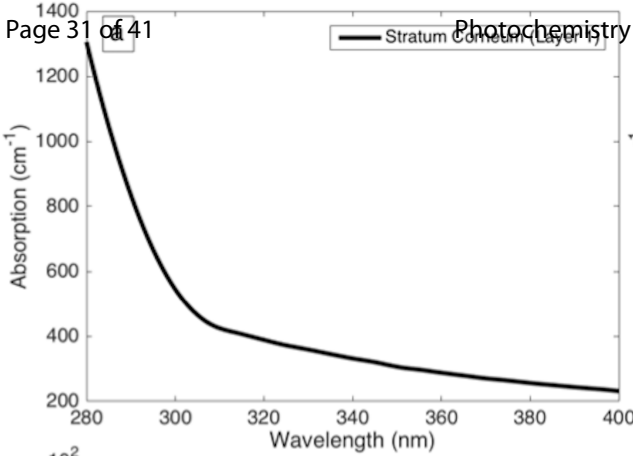
a
Stratum Corneum (Layer 1)
Absorption (cm^{-1})
Wavelength (nm)

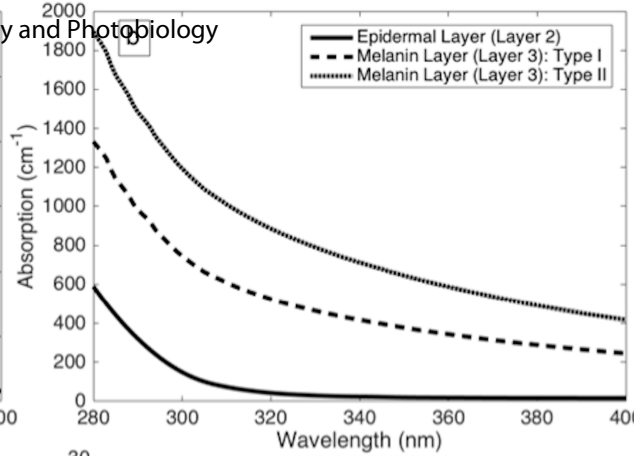
b
Epidermal Layer (Layer 2)
Melanin Layer (Layer 3): Type I
Melanin Layer (Layer 3): Type II
Absorption (cm^{-1})
Wavelength (nm)

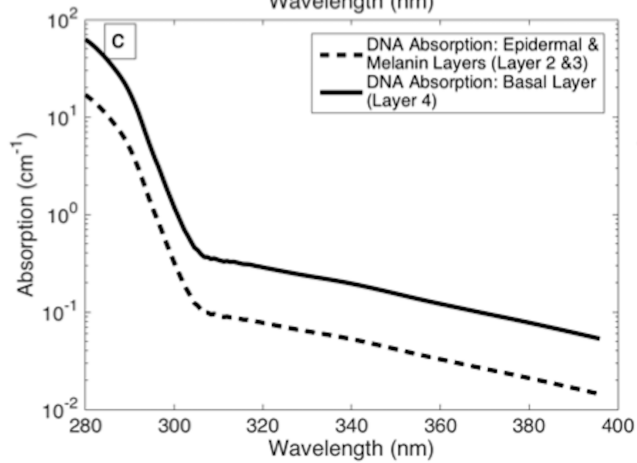
c
DNA Absorption: Epidermal & Melanin Layers (Layer 2 &3)
DNA Absorption: Basal Layer (Layer 4)
Absorption (cm^{-1})
Wavelength (nm)

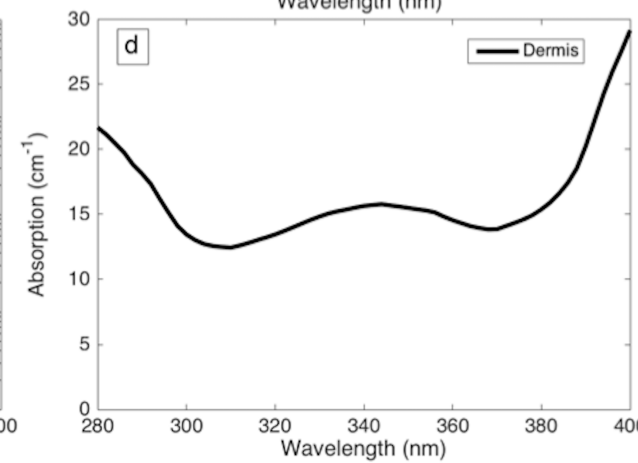
d
Dermis
Absorption (cm^{-1})
Wavelength (nm)

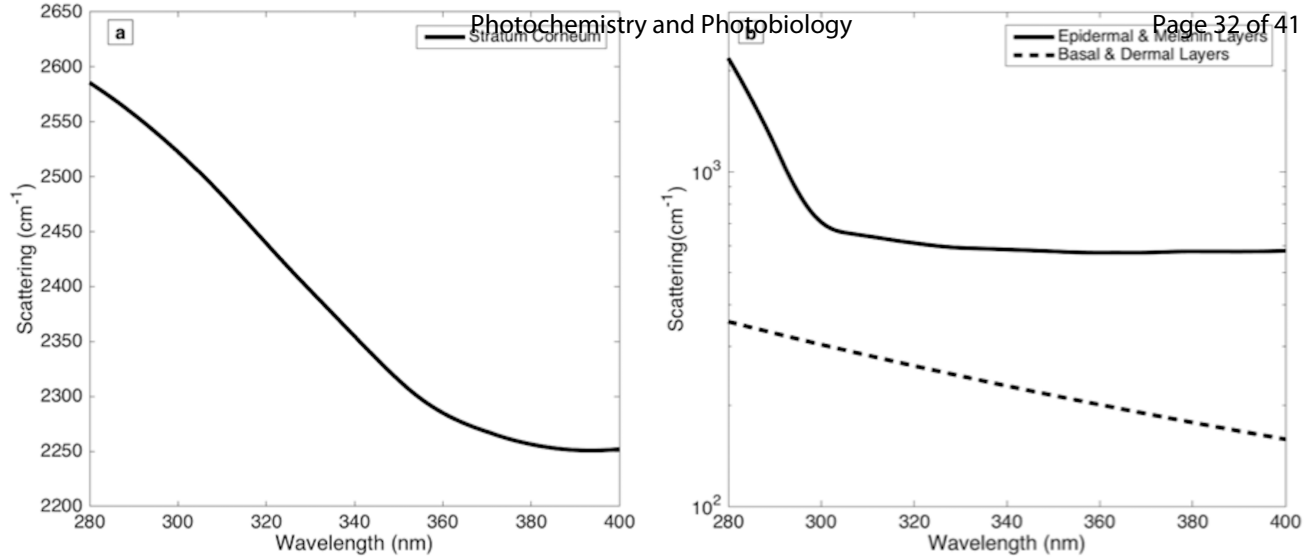
a
Stratum Corneum
Scattering (cm-1)
Wavelength (nm)
b
Epidermal & Melanin Layers
Basal & Dermal Layers
Scattering(cm-1)
Wavelength (nm)

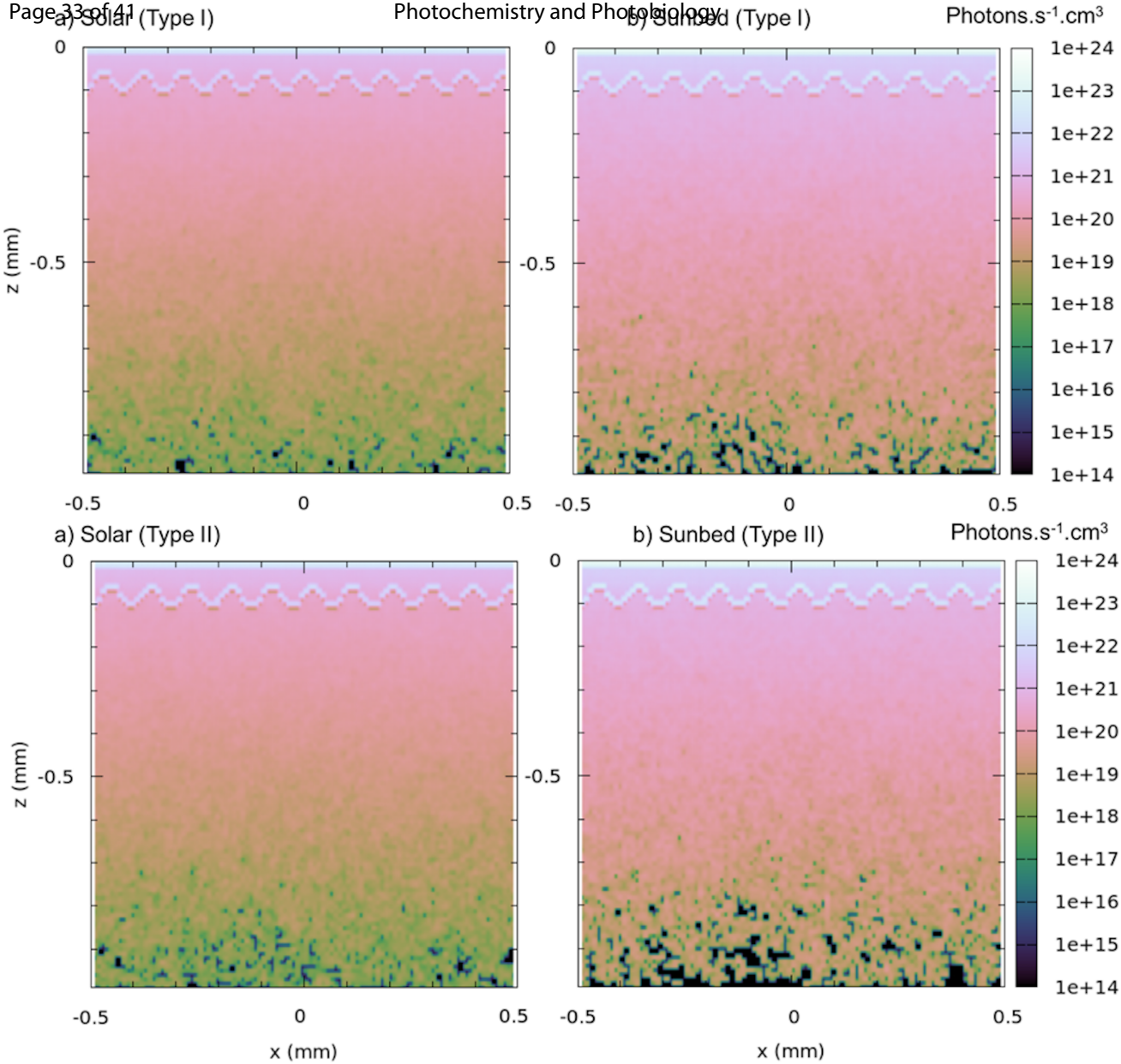
a) Solar (Type I)
b) Sunbed (Type I)
Photons.s-1.cm3
1e+24
1e+23
1e+22
1e+21
1e+20
1e+19
1e+18
1e+17
1e+16
1e+15
1e+14
z (mm)
0
-0.5
-0.5
0
0.5
a) Solar (Type II)
b) Sunbed (Type II)
Photons.s-1.cm3
x (mm)

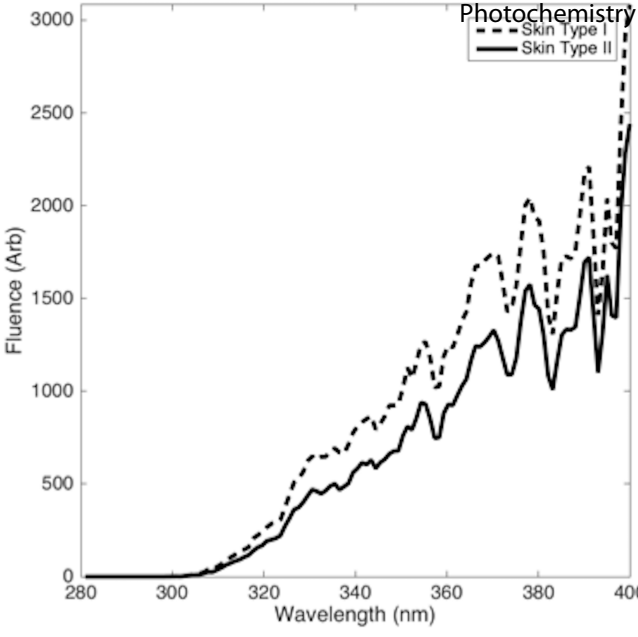
Skin Type I
Skin Type II
Fluence (Arb)
Wavelength (nm)
0
500
1000
1500
2000
2500
3000
280
300
320
340
360
380
400

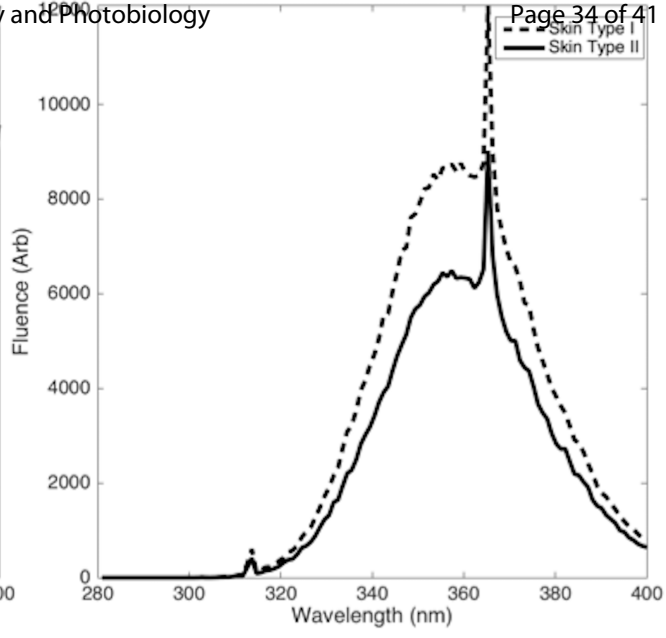
Skin Type I
Skin Type II
Fluence (Arb)
Wavelength (nm)
0
2000
4000
6000
8000
10000
280
300
320
340
360
380
400